Analysis of the kinetics for the $H_2 + \frac{1}{2}O_2 \rightleftharpoons H_2O$ reaction on a hot Pt surface in the pressure range 0.10–10 Torr

Michael Försth [a,*], Frank Eisert [b], Fredrik Gudmundson [a], John Persson [a] and Arne Rosén [a]

[a] *Department of Experimental Physics, Chalmers University of Technology and Göteborg University, SE-41296 Göteborg, Sweden*
E-mail: forsth@fy.chalmers.se
[b] *Institut für Angewandte Physikalische Chemie, INF253, D-69120 Heidelberg, Germany*

Received 18 January 2000; accepted 17 March 2000

The $H_2 + \frac{1}{2}O_2 \rightleftharpoons H_2O$ reaction on platinum at 700 and 1300 K has been studied. A stagnation flow geometry was used with a gas mixture of H_2 and O_2 at pressures between 0.10 and 10 Torr. Comparing SHG results with simulations using different reaction parameters, it was concluded that $E^{f}_{H_2O} \approx 0.7$ eV, $E^{f}_{OH} \approx 0.7$ eV, and $E^{d}_{OH} \approx 2.6$ eV. LIF measurements showed an ambiguity in the choice of main water-producing channel. Both hydrogen addition with low sticking coefficients and hydroxyl disproportionation with high sticking coefficients are plausible.

Keywords: platinum, hydrogen oxidation, water production, surface chemistry, LIF, SHG, CHEMKIN

1. Introduction

The catalytic combustion of hydrogen on Pt is one of the most studied heterogeneous catalytic processes [1]. The reason for this is that H_2 and O_2 yield a rather simple chemistry with few adsorbates, O_2 being the heaviest, although there have been suggestions that heavier molecules also could exist on the surface [2]. If the species being oxidized is changed from hydrogen to a simple hydrocarbon such as methane, the number of pure surface reactions increases from three [3] to nine [4], assuming dissociative sticking in both cases. By pure surface reaction is meant a reaction where only adsorbed surface species participate, that is, no gas-phase species participate. Despite the relative simplicity of the reaction, there is still a lack of knowledge about reaction rate parameters for the surface reactions involved, as well as about which are the most important surface reactions. Important parameters for the overall water production on the surface are the sticking coefficients $s_0(H_2)$ and $s_0(O_2)$ for hydrogen and oxygen, that is, the probability for the molecules to adsorb on the surface when they impinge on it [5,6].

In general, when studying the interaction between surface and gas phase it is most often the adsorption/desorption reactions that are rate-limiting, not the surface reactions [7]. In order to study the surface chemistry, except for adsorption and desorption, it is therefore necessary to focus on intermediate steps in the reaction, and not on the overall process, the latter being the case in, for example, microcalorimetry. In this work the coverage of oxygen atoms on the surface has been studied with second harmonic generation, SHG, which allows us to discriminate between high and low activation energies [8,9]. In order to determine which of the water production paths $H_a + OH_a \rightleftharpoons H_2O_a$, hydrogen addition, and $2OH_a \rightleftharpoons H_2O_a + O_a$, hydroxyl disproportionation, is the most important, the desorbed OH in the gas close to the surface has been studied with laser-induced fluorescence, LIF.

In [10] the activation energy for the reaction $H_a + OH_a \rightarrow H_2O$ is found to be $E^{f_1}_{H_2O} = 0.67$ eV, while the activation energy for the reaction $2OH_a \rightarrow H_2O_a + O_a$ is $E^{f_2}_{H_2O} = 0.75$ eV. The experimental technique was modulated molecular beam relaxation spectroscopy, MMBRS, and the isotope deuterium was used instead of hydrogen in order to avoid signal interference from background H_2O. The difference between deuterium and hydrogen was expected to be negligible in the context of the studied parameters. The experimental data give less information about the activation energy for OH formation, E^{f}_{OH}, but the authors concluded that an upper limit is $E^{f}_{OH} \leqslant 0.57$ eV.

In [11] the activation energy for the reaction $2OH_a \rightarrow H_2O_a + O_a$ was found to be $E^{f_2}_{H_2O} = 0.18$ eV, while the activation energy for OH formation, $O + H_a \rightarrow OH_a$ was found to be $E^{f}_{OH} = 0.12$ eV. The experimental technique was time-resolved electron energy loss spectroscopy, TREELS. It was found that the value obtained for $E^{f}_{H_2O}$ was relatively independent of the reaction path, hydroxyl disproportionation or hydrogen addition, and therefore 0.18 eV may also be considered as an estimation of $E^{f_1}_{H_2O}$.

Formation and decomposition of water on a Pt(111) surface were studied with LIF in [12], and an enthalpy diagram for hydrogen oxidation was discussed in detail. It was observed in [12] and [13] that the difference between the activation energies for hydroxyl desorption and for water formation, $E^{d}_{OH} - E^{f_1}_{H_2O}$, is not uniquely determined. The reason why the experimental data are not sufficient to determine these activation energies independently is that the

* To whom correspondence should be addressed.

desorption of OH, which is what is probed by the LIF experiments, depends on the ratio between the expressions for OH desorption and H_2O formation, since a high yield of H_2O will decrease the OH coverage, and therefore also the OH desorption rate. With the experimental data the authors arrive at a difference $E^{\mathrm{d}}_{\mathrm{OH}} - E^{\mathrm{f_1}}_{\mathrm{H_2O}} = 1.9$ eV.

As a result of these works the proposed activation energies can be divided into two groups. One group has relatively high energies: $E^{\mathrm{f}}_{\mathrm{H_2O}} \approx 0.7$ eV, $E^{\mathrm{f}}_{\mathrm{OH}} \approx 0.7$ eV, and $E^{\mathrm{d}}_{\mathrm{OH}} \approx 2.6$ eV. The other group contains a set of lower activation energies: $E^{\mathrm{f}}_{\mathrm{H_2O}} \approx 0.18$ eV, $E^{\mathrm{f}}_{\mathrm{OH}} \approx 0.12$ eV, and $E^{\mathrm{d}}_{\mathrm{OH}} \approx 2.1$ eV.

Another point of interest is which of the water production paths $H_a + OH_a \rightleftharpoons H_2O_a$, hydrogen addition, and $2OH_a \rightleftharpoons H_2O_a + O_a$, hydroxyl disproportionation, is the most important one. This is not uniquely determined by their activation energies $E^{\mathrm{f_1}}_{\mathrm{H_2O}}$ and $E^{\mathrm{f_2}}_{\mathrm{H_2O}}$, respectively, but also depends on pre-exponentials and coverages of surface species, among other factors.

In [10] it is concluded that $H_a + OH_a \rightleftharpoons H_2O_a$ is the dominant path when hydrogen flux to the surface exceeds that of oxygen, and that $2OH_a \rightleftharpoons H_2O_a + O_a$ dominates when the oxygen flux exceeds that of hydrogen. A kinetic analysis [13] showed that the relative importance of the two reaction paths could depend sensitively on temperature and on α, which is the relative hydrogen pressure, $\alpha = p_{\mathrm{H_2}}/(p_{\mathrm{O_2}} + p_{\mathrm{H_2}})$. Hydrogen addition is favored by high temperatures and high α, while the hydroxyl disproportionation path is more favored at low temperatures and low α, which means oxygen excess.

The present study aims at discriminating between the four combinations of high or low activation energies with the hydrogen addition or the hydroxyl disproportionation path.

2. Material and method

The stagnation-point flow field studied in this work is shown in figure 1. At a certain distance below the plane of the surface, in the gas phase, an upward velocity is imposed. By confining our attention to the center of the surface, edge effects can be neglected, permitting use of a one-dimensional analysis. In the pressure range from 0.10 to 10 Torr, relevant for this study, the mean free path of the molecules decreases from around 500 μm to around 5 μm at 300 K, increasing linearly with the temperature. The temperature of the surface is a boundary condition in the calculations and is experimentally kept fixed by adaptive resistive heating.

2.1. Experimental techniques

The cleanliness of the surfaces is known to be of high importance for the kinetics of the surface reaction [14]. Therefore, it is important to use a reliable cleaning method

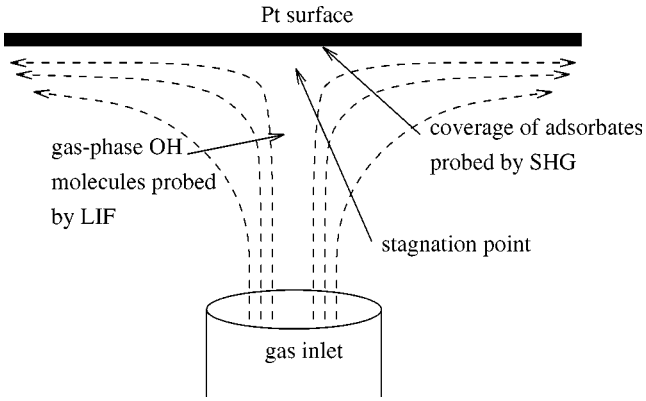

Figure 1. Stagnation-point flow.

which guarantees a reproducible cleanliness in the experiments. For the $H_2 + \frac{1}{2}O_2 \rightleftharpoons H_2O$ reaction on Pt it has been shown [14] that the reaction itself produces a clean surface, and this was also the method used for both the SHG and the LIF experiments.

2.1.1. SHG

A detailed description of the SHG experimental setup is given in [15]. The SHG experiments were performed in a small turbopumped UHV chamber. In order to obtain stagnation-point flow conditions, care was taken to provide a flat velocity profile by stacking glass beads, enclosed by a metal mesh, in the inlet tube shown at the bottom of figure 1. Measurements were made for the pressures 0.20, 1.0, and 10 Torr and the temperature of the resistively heated Pt(111) surface was 700 K. A mode-locked Nd:YAG laser, $\lambda = 1064$ nm, with a pulse length of 35 ps at a repetition rate of 10 Hz was used. Consequently, the frequency-doubled light, created by the second-order susceptibilities of the surface and the surface/adsorbate complex, had a wavelength of 532 nm. Theoretical foundations for the interpretation of the SHG signal as a measure of the coverage, θ, of adsorbates are given in, for example, [15] and [8].

2.1.2. LIF

A detailed description of the LIF experimental setup is given in, for example, [6]. The LIF experiments were performed in a roots-pumped vacuum chamber. The velocity profile from the inlet tube was not flat. However, as we focussed on the central, maximum-velocity parts of the flow, the experimental conditions were well known. A detailed discussion of the flow geometry in this experiment is given in [16]. Measurements were made for the pressures 0.10, 0.50, and 1.0 Torr and the temperature of the resistively heated polycrystalline Pt surface was 1300 K. A frequency-doubled excimer-pumped dye laser was tuned to the $R_1(4)$ transition, $\lambda = 307$ nm, in the OH molecule. A major concern in LIF is quenching [17]. There are three parameters that influence the quenching rate: pressure, temperature, and gas composition. In figure 8 the OH-LIF intensities are normalized to unity at their maxima. Since the pres-

sure is constant for each curve this parameter, pressure, does not influence them.

Temperature, and therefore the absolute density, can also influence the quenching rate. However, for pressures $p_{\text{tot}} \leqslant 1.0$ Torr the temperature profile outside the surface should not vary considerably for a data set with constant pressure, since no gas-phase reactions take place [18].

What may influence the appearance of the curves in figure 8 is the gas composition. Water is a more efficient quencher than hydrogen and oxygen molecules. Therefore, the changes in water concentration may influence the shape of the curves. The largest quenching and variation in quenching occur for the highest pressure, $p_{\text{tot}} = 1.0$ Torr. For $\alpha = 0.1$ the measured quenching rate was 3.0×10^6 s^{-1} based on OH lifetime measurements [18]. Using the tabulated cross sections for $T = 1100$ K [19] it is estimated that the maximum quenching rate variation could be 2.8–3.5 $\times$ 10^6 s^{-1} for α ranging from 0.0 to 0.4 at $p_{\text{tot}} = 1.0$ Torr. This would mean a maximal positive correction of +9% of the magnitude in OH concentration for $\alpha = 0.25$–0.30, and a maximal negative correction of −5% for $\alpha = 0$. The corrections for $p_{\text{tot}} = 0.5$ Torr will be a factor of two smaller, and for $p_{\text{tot}} = 0.1$ Torr the corrections will be an order of magnitude smaller. On the whole, we consider the quenching variations small enough to be neglected.

2.2. Theoretical modeling

2.2.1. Mass-transfer limitation

Before analyzing and comparing the experimental and simulated results as a function of reactant composition, it is necessary to know if and how the reactant composition at the gas inlet, which is determined by the flowmeters, differs from the reactant composition at the boundary layer close to the surface. The change in composition along the way from the inlet to the surface can be due to two factors:

Mass-transport limitation. In this case the surface reactions consume one or more of the reactants at a rate such that they are depleted in the gas near the surface. This might happen even if the reactant mixture at the inlet is stoichiometric, from the surface reaction point of view, because of different diffusion velocities for the different reactants.

Gas-phase chemistry. If gas-phase reactions take place it is evident that the gas composition will change during the transport from the inlet to the surface. Products will appear and reactants will be consumed.

In this study the mass-transport limitation will be of importance while the gas-phase chemistry will be less important. It has been shown [18] that for the LIF-experiment conditions, $T = 1300$ K, gas-phase chemistry is negligible for pressures up to 1 Torr, which is the highest pressure used for LIF experiments in this study.

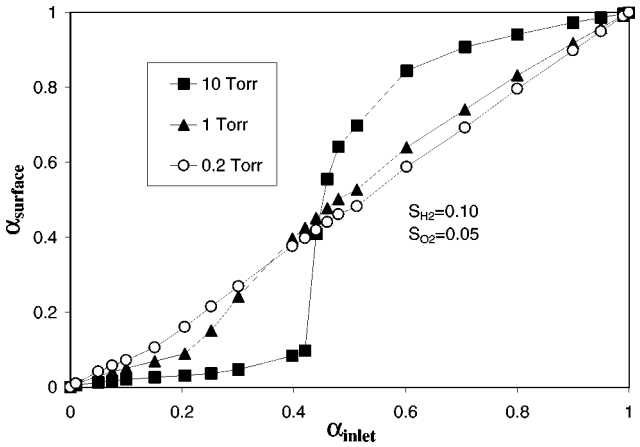

Figure 2. Mass-transport effects at 700 K. The simulations were made with Chemkin.

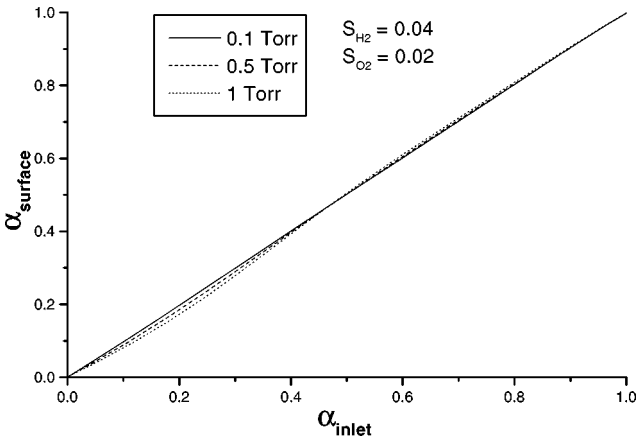

Figure 3. Mass-transport effects at 1300 K. The simulations were made with Chemkin.

The mass-transport effect for the SHG-experiment conditions, $T = 700$ K, is shown in figure 2. The effect seems to be more pronounced than in figure 3, which shows the mass-transport effect for the LIF-experiment conditions at 1300 K, mainly because the highest pressure is 10 Torr in figure 2, compared to 1 Torr in figure 3. Figure 2 shows the dependence of α_{surface}, that is, $p_{H_2}/(p_{H_2} + p_{O_2})$ in the gas phase close to the surface, as a function of hydrogen partial pressure at the inlet, α_{inlet}, for the conditions of the SHG experiment, $T = 700$ K. Hence, the figure shows that for lean mixtures, that is, low α_{inlet}, the hydrogen is depleted close to the surface because of the finite diffusion and convection velocities. The opposite is true for the rich mixtures, that is, high α_{inlet}. However, due to the difference in minority species, the mass-transport is more important for lean mixtures, that is, low α_{inlet}, than for rich mixtures. This is also evident in figure 3 where the effect is more pronounced for low than for high α_{inlet}.

It should be noticed that there is a clear difference in shape between the curve for 0.1 Torr and the curve for 10 Torr in figure 2. This is because, at $T = 700$ K, the mean free path of the molecules decreases from around 1 mm at $p = 0.1$ Torr to around 10 μm at 10 Torr, as dis-

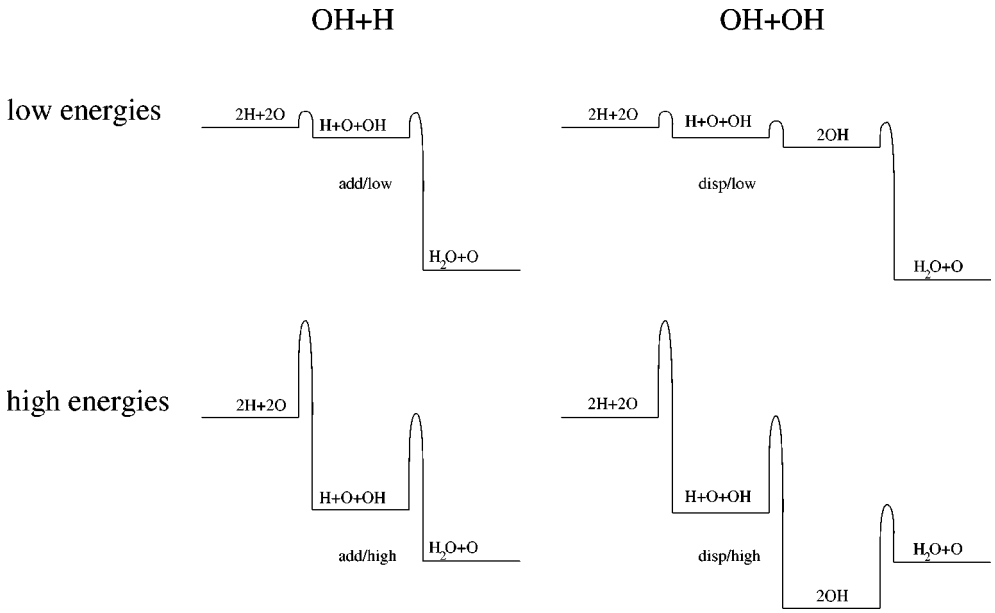

Figure 4. The two different reaction paths with different activation energies: add/low, add/high, disp/low, and disp/high. The hydrogen addition path, $OH + H \rightleftharpoons H_2O$, is denoted "add", while the disproportionation path, $OH + OH \rightleftharpoons H_2O + O$, is denoted "disp". For the low-energy models, add/low and disp/low, the activation energy is $E^{f}_{OH} = 0.12$ eV for OH formation, $E^{f}_{H_2O} = 0.18$ eV for water formation, and $E^{d}_{OH} = 2.1$ eV for OH desorption. For the high-energy models, add/high and disp/high, the corresponding activation energies are: $E^{f}_{OH} = 0.7$ eV, $E^{f}_{H_2O} = 0.7$ eV, and $E^{d}_{OH} = 2.6$ eV.

cussed above. Thus, the flow passes from near molecular flow to near viscous flow. It is in this intermediate flow regime that the mass-transport starts to be limiting for the surface reaction.

In figures 2 and 3 the sticking coefficients are chosen as $s_0(H_2)/s_0(O_2)$ equal to $0.10/0.05$ and $0.04/0.02$, respectively. Along with these sticking coefficients a set of relatively high coefficients, $s_0(H_2)/s_0(O_2) = 0.18/0.09$ will also be investigated in this study, see below. The relation between $\alpha_{surface}$ and α_{inlet} depends significantly on the sticking coefficients chosen.

The difference between α_{inlet} and $\alpha_{surface}$, where

$$\alpha_{inlet} = \frac{p_{H_2,inlet}}{p_{H_2,inlet} + p_{O_2,inlet}}$$

and

$$\alpha_{surface} = \frac{p_{H_2,surface}}{p_{H_2,surface} + p_{O_2,surface}},$$

has to be taken into account when we plot experimental values as a function of $\alpha_{surface}$, as in figures 5, 6, and 7.

2.2.2. Simulations

Two types of simulations were used. In order to correctly describe the relation between gas compositions at the inlet and at the surface, as described below, the Chemkin package was employed. Using the codes CHEMKIN [20], SPIN [21], SURFACE CHEMKIN [22], TRANSPORT [23], thermodynamic data base [24], and TWOPNT [25], the coupled gas-phase and surface-phase chemistries could be simulated. A detailed description of the coupled gas-phase and surface-phase chemistries, and of the Chemkin simulations, is given in [6].

For the simulations of oxygen and hydroxyl coverage, θ(O) and θ(OH), as a function of gas mixture, a surface model without gas-phase chemistry was used. This model, the HKZ-model developed by Hellsing, Kasemo and Zhdanov [13], calculates the coverages of all species in the $H_2 + \frac{1}{2}O_2 \rightleftharpoons H_2O$ reaction. It requires much less computation time since the gas-phase chemistry is not incorporated. The method for simulating the system has thus been first to use the Chemkin package in order to establish the gas composition above the surface, given a certain inlet reactant mixture, and then to use the pure surface model to test the studied parameters for the reaction. The discriminations to be made, discussed in section 1, are: hydrogen addition versus hydroxyl disproportionation path, and high versus low activation energies. These four alternative models are summarized in figure 4.

3. Results and discussion

3.1. SHG experiments and modeling of oxygen coverage

Oxygen coverage, θ(O), for the pressures 0.20, 1.0, and 10 Torr is presented in figures 5, 6, and 7, respectively. The discrete datapoints marked with diamonds ($\diamondsuit$) represent experimental θ(O) according to SHG experiments. The curves drawn with dashed, fine solid, and thick solid lines represent the simulated θ(O) with the reaction models add/high, disp/high and either of add/low or disp/low, respectively. The hydrogen addition path, $OH + H \rightleftharpoons H_2O$, is denoted "add", while the disproportionation path, $OH + OH \rightleftharpoons H_2O + O$, is denoted "disp". Also, "high" and "low" refer to high or low activation energies, respectively, see also figure 4. The coverage is given as a function of $\alpha_{surface}$. The

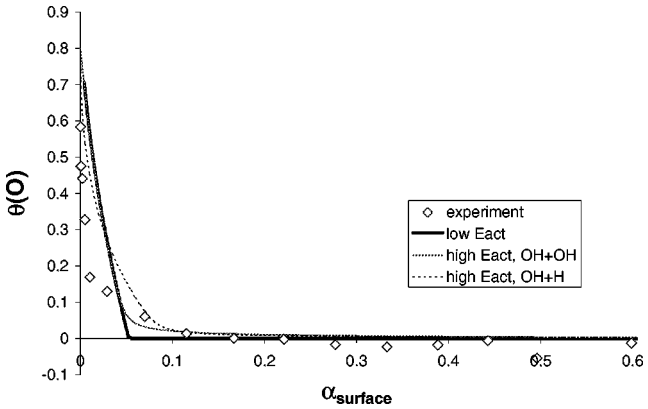

Figure 5. Pressure $p_{\text{tot}} = 0.20$ Torr. Comparison of experimental oxygen coverage, θ(O), obtained with SHG, and theoretically predicted θ(O) obtained with the kinetic surface model, with three different parameter sets.

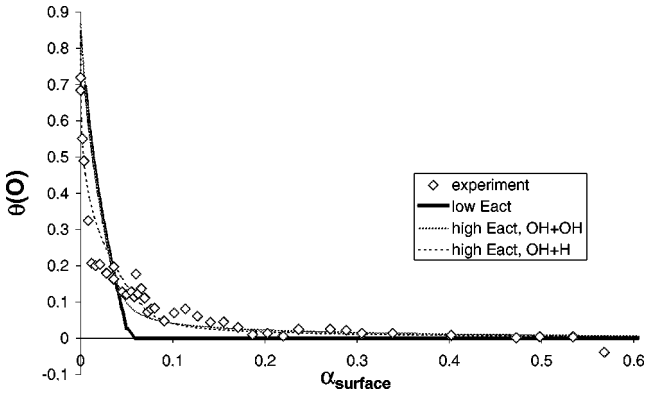

Figure 6. Pressure $p_{\text{tot}} = 1.0$ Torr. Comparison of experimental oxygen coverage, θ(O), obtained with SHG, and theoretically predicted θ(O) obtained with the kinetic surface model, with three different parameter sets.

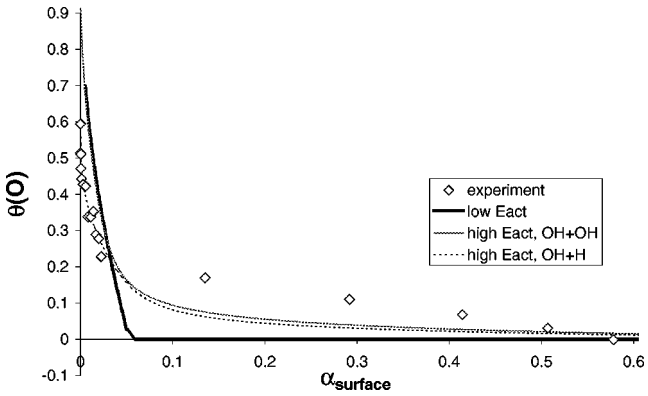

Figure 7. Pressure $p_{\text{tot}} = 10$ Torr. Comparison of experimental oxygen coverage, θ(O), obtained with SHG, and theoretically predicted θ(O) obtained with the kinetic surface model, with three different parameter sets.

agreement between experiment and theory is not perfect for any reaction model. Most evident is that the "tail" in θ(O) is definitely not reproduced by the (add or disp)/low model, which drops to a minimum very rapidly for all three pressures. This initial fast drop of the oxygen coverage, with increasing α, is a result of the low activation energies, and does not depend on reaction path. Hence, the solid line in figures 5, 6, and 7 correspond to both add/low and disp/low. Figure 7 which shows the results for 10 Torr gives the clearest evidence that the (add or disp)/low does not correctly describe the experimental reality. Therefore, the possibility of low activation energies can be ruled out. However, whether model add/high or disp/high is the most important one cannot be concluded from the SHG results. Nevertheless, it has been found [15] that for very low hydrogen partial pressures, $\alpha \leqslant 0.03$, only the hydrogen addition path is able to correctly model the oxygen coverage. The hydroxyl disproportionation path predicts too high oxygen coverages in this α-range, and it is therefore excluded in [15]. In order to investigate the reaction path from a more general point of view, and not only for very low α, the LIF experiments are referred to as explained below.

3.2. LIF experiments and modeling of hydroxyl coverage

Since the SHG measurements, together with simulations, indicate that the activation energies are high, add/high and disp/high are the remaining candidates. In order to decide whether $OH + H \rightleftharpoons H_2O$ or $OH + OH \rightleftharpoons H_2O + O$ is the main reaction path we use the LIF results in figure 8 and compare them with the simulated results in figure 9. These figures show the normalized simulated coverage of OH, θ(OH), on the surface for the pair of sticking coefficients $s_0(H_2)/s_0(O_2)$ equal to $0.04/0.02$, $0.10/0.05$, and $0.18/0.09$, respectively. All experimental and simulated data are normalized to unity at their maximum. One might question the comparison between gas-phase OH, probed by LIF, and the simulated OH coverage, θ(OH). However, under the conditions of the LIF experiment, $p_{\text{tot}} \leqslant 1$ Torr and $T = 1300$ K, gas-phase chemistry should be negligible [18] and, therefore, the gas-phase OH concentration should be proportional to the OH desorption, which should be proportional to the coverage.

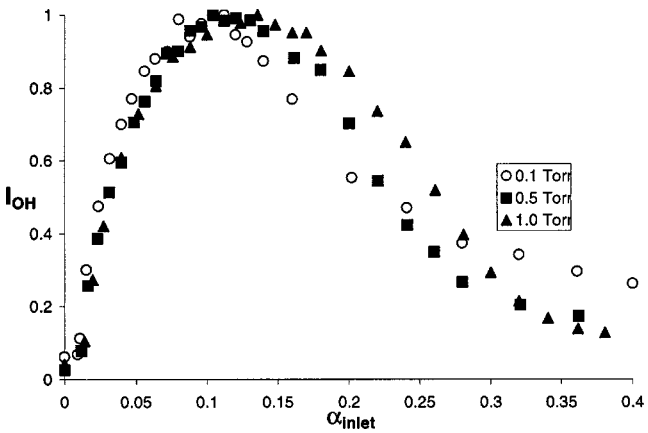

Figure 8. Experimentally obtained OH-LIF intensity. For each pressure the maximum intensity has been normalized to unity at their maximum.

The first feature that should be noticed when studying the experimental data in figure 8 is that the α_{inlet} value for which the fluorescence is maximal increases with increasing

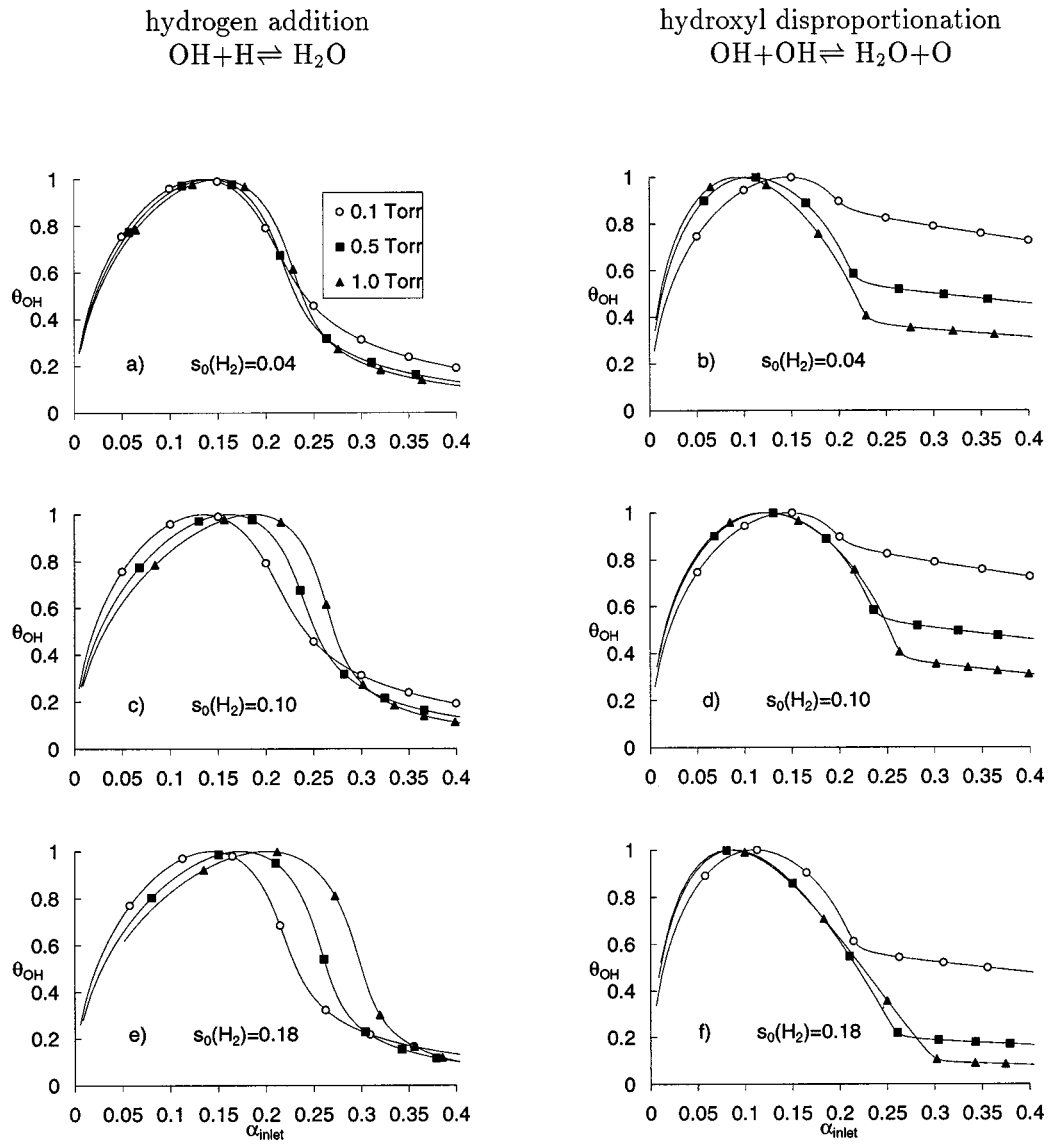

Figure 9. Comparison of simulated OH coverage, θ(OH), for six different combinations of sticking coefficients and reaction paths. The first row, (a) and (b), shows the simulated results for the sticking coefficients $s_0(H_2)/s_0(O_2) = 0.04/0.02$, with the hydrogen addition path $OH + H \rightleftharpoons H_2O$ as unique water-producing reaction channel to the left (a), and with the hydroxyl disproportionation path $OH + OH \rightleftharpoons H_2O + O$ as unique water-producing reaction channel to the right (b). The second and third rows, (c) and (d), and (e) and (f), contain simulated results with $s_0(H_2)/s_0(O_2)$ equal to $0.10/0.05$ and $0.18/0.09$, respectively.

pressure. This is mainly due to the increasing mass-transfer limitation of hydrogen supply described above, which depletes the H_2 concentration close to the surface, yielding a local α_{surface} which is lower than the α_{inlet} at the gas inlet, see figure 3. This behavior is reproduced by the hydrogen addition path, $OH + H \rightleftharpoons H_2O$. The best agreement is obtained using relatively low sticking coefficients, $s_0(H_2)/s_0(O_2) \leqslant 0.10/0.05$. The hydroxyl disproportionation path, $OH + OH \rightleftharpoons H_2O + O$, does not reproduce this behavior, as is evident from figure 9.

The simulations of the disproportionation path contradict the experimental results, since in figure 9 (b), (d), and (f), the maximum coverage shifts to higher α_{inlet} as the pressure *decreases*, whereas in the experimental results, figure 8, the maximum shifts to higher α_{inlet} as the pressure *increases*. However, the discrepancy between the disproportionation path and the experimental results decreases in magnitude with increasing sticking coefficients since this opposite shift becomes less pronounced for high sticking coefficients. Furthermore, the position on the α-axis where the OH-maximum occurs is poorly reproduced by the hydrogen addition path while it is fairly well reproduced by the hydroxyl disproportionation path. Again this is especially true for high sticking coefficients. On the other hand, another complication of the hydroxyl disproportionation path is the relatively abrupt transition from a fast to a slower linear decay that occurs for α_{inlet} between 0.2 and 0.3. This transition does not exist in the experimental data in figure 8, nor in the simulations of the hydrogen addition path.

Summarizing, the hydrogen addition path, $OH + H \rightleftharpoons H_2O$, with relatively low sticking coefficients, reproduces the increase in α-position for maximum OH with increasing pressure. On the other hand, the hydroxyl disproportionation path, $OH + OH \rightleftharpoons H_2O + O$, with relatively high sticking coefficients, reproduces the absolute position on the α-axis for maximum OH more precisely than the hydrogen addition path does, although the shape of the disproportionation curves looks different than the shape of the experimental curves. On the whole this leaves an ambiguity in the answer to which of the two reaction paths is the most important.

4. Conclusions

The $H_2 + \frac{1}{2}O_2 \rightleftharpoons H_2O$ reaction on heated platinum surfaces has been examined in a combined SHG, LIF, Chemkin, and surface model study. From SHG studies of oxygen coverage on a Pt(111) surface at 700 K it was concluded that the activation energies for H_2O and OH production, and OH desorption, should agree best with the higher ones previously reported in the literature, $E^{\mathrm{f}}_{\mathrm{H_2O}} \approx 0.7$ eV, $E^{\mathrm{f}}_{\mathrm{OH}} \approx 0.7$ eV, and $E^{\mathrm{d}}_{\mathrm{OH}} \approx 2.6$ eV. The SHG experiments, however, could not give any information whether the hydrogen addition path, $OH + H \rightleftharpoons H_2O$, or the disproportionation path, $2OH \rightleftharpoons H_2O + O$, is the main reaction path. This problem was approached with LIF studies of OH above a polycrystalline Pt surface at 1300 K which indicated an ambiguity in the model. It is not possible to determine with certainty which of the two alternatives, hydrogen addition with relatively low sticking coefficients, $s_0(H_2)/s_0(O_2) \leqslant 0.10/0.05$, or hydroxyl disproportionation with relatively high sticking coefficients, $s_0(H_2)/s_0(O_2) \geqslant 0.10/0.05$, is the main reaction path.

In order to understand the water-production mechanism in detail, more precise measurements of the sticking coefficients are necessary. Literature data on the hydrogen sticking coefficient $s_0(H_2)$, for example, are quite scattered. They range from 0.04 [5,26] to 0.16 [27] and up to 0.28 [12] for a flat heated Pt surface.

Acknowledgement

We gratefully acknowledge financial support from Volvo Research Foundation and Volvo Educational Foundation (contract No. 92:36), the Swedish Natural Science Research Council (NFR, contract No. E-EG 2560-129), the Swedish Research Council for Engineering Sciences (TFR, contract No. 92-538), and Combustion Engine Research Institute (CERC).

References

[1] P.R. Norton, in: *The Chemical Physics of Solid Surfaces and Heterogeneous Catalysis*, Vol. 4, eds. D.A. King and D.P. Woodruff (Elsevier, Amsterdam, 1982) pp. 27–72.
[2] L.K. Verheij, M. Freitag, M.B. Hugenschmidt, I. Kempf, B. Poelsema and G. Comsa, Surf. Sci. 272 (1992) 276.
[3] J. Warnatz, M.D. Allendorf, R.J. Kee and M.E. Coltrin, Combust. Flame 96 (1994) 393.
[4] O. Deutschmann, F. Behrendt and J. Warnatz, Catal. Today 21 (1994) 461.
[5] S. Ljungström, B. Kasemo, A. Rosén, T. Wahnström and E. Fridell, Surf. Sci. 216 (1989) 63.
[6] M. Försth, F. Gudmundson, J.L. Persson and A. Rosén, Combust. Flame 119 (1999) 144.
[7] F. Behrendt, O. Deutschmann, U. Maas and J. Warnatz, J. Vac. Sci. Technol. 13A (1995) 1373.
[8] F. Eisert, A. Elg and A. Rosén, Appl. Phys. A 60 (1995) 209.
[9] F. Eisert and A. Rosén, Phys. Rev. B 54 (1996) 14061.
[10] A.B. Anton and D.C. Cadogan, J. Vac. Sci. Technol. 9A (1991) 1890.
[11] T.A. Germer and W. Ho, Chem. Phys. Lett. 163 (1989) 449.
[12] E. Fridell, A.-P. Elg, A. Rosén and B. Kasemo, J. Chem. Phys. 102 (1995) 5827.
[13] B. Hellsing, B. Kasemo and V.P. Zhdanov, J. Catal. 132 (1991) 210.
[14] K.-E. Keck and B. Kasemo, Surf. Sci. 167 (1986) 313.
[15] F. Eisert, F. Gudmundson and A. Rosén, Appl. Phys. B 68 (1999) 579.
[16] F. Gudmundson, Ph.D. thesis, Chalmers University of Technology and Göteborg University (1998).
[17] A.C. Eckbreth, *Laser Diagnostics for Combustion Temperature and Species*, 2nd Ed. (Gordon and Breach, New York, 1996).
[18] F. Gudmundson, J.L. Persson, M. Försth, F. Behrendt, B. Kasemo and A. Rosén, J. Catal. 179 (1998) 420.
[19] P.W. Fairchild, G.P. Smith and D.D. Crosley, J. Chem. Phys. 79 (1983) 1795.
[20] R.J. Kee, F.M. Rupley and J.A. Miller, Chemkin-II: A Fortran Chemical Kinetics Package for the Analysis of Gas Phase Chemical Kinetics, Sandia National Laboratories Report SAND89-8009B, Albuquerque, NM/Livermore, CA (1989).
[21] M.E. Coltrin, R.J. Kee, G.H. Evans, E. Meeks, F.M. Rupley and J.F. Grcar, SPIN (Version 3.83): A Fortran Program for Modelling One-Dimensional Rotating-Disk/Stagnation-Flow Chemical Vapor Deposition Reactors, Sandia National Laboratories Report SAND91-8003, Albuquerque, NM/Livermore, CA (1991).
[22] M.E. Coltrin, R.J. Kee and F.M. Rupley, SURFACE CHEMKIN (Version 4.0): A Fortran Package for Analyzing Heterogeneous Chemical Kinetics at a Solid-Surface–Gas-Phase Interface, Sandia National Laboratories Report SAND90-8003B, Albuquerque, NM/Livermore, CA (1990).
[23] R.J. Kee, G. Dixon-Lewis, J. Warnatz, M.E. Coltrin and J.A. Miller, A Fortran Computer Code Package for the Evaluation of Gas-Phase Multicomponent Transport Properties, Sandia National Laboratories Report SAND86-8246, Albuquerque, NM/Livermore, CA (1986).
[24] R.J. Kee, F.M. Rupley and J.A. Miller, The Chemkin Thermodynamic Data Base, Sandia National Laboratories Report SAND87-8215B, Albuquerque, NM/Livermore, CA (1987).
[25] J.F. Grcar, The Twopnt Program for Boundary Value Problems, Sandia National Laboratories Report SAND91-8230, Albuquerque, NM/Livermore, CA (1991).
[26] A.-P. Elg, F. Eisert and A. Rosén, Surf. Sci. 382 (1997) 57.
[27] M. Salméron, R.J. Gale and G.A. Somorjai, J. Chem. Phys. 70 (1979) 2807.